Journal of Sound and Vibration (1997) **207**(5), 647–669

ON THE FREE VIBRATION OF COMPLETELY FREE, OPEN, CYLINDRICALLY CURVED, ISOTROPIC SHELL PANELS

N. S. Bardell†, J. M. Dunsdon and R. S. Langley

Department of Aeronautics and Astronautics, University of Southampton, Highfield, Southampton SO17 1BJ, England

(*Received* 17 *May* 1996, *and in final form* 14 *May* 1997)

The *h-p* version of the finite element method is used to furnish a detailed study of the vibration characteristics of completely free, open, cylindrically curved, isotropic shell panels. Convergence studies have been carried out to ascertain the most appropriate mix of *h*-refinement and *p*-enrichment necessary to give a reasonable solution accuracy; this approach has been corroborated by comparing results from the present methodology with the work of other investigators and the results forthcoming from a proprietary finite element package. Extensive results have been presented for panels with aspect ratios of 0·5, 1 and 2, the curvature of which is gradually increased from that of a flat plate at one extreme, to a complete, although unjoined, cylinder at the other. Curves of frequency versus included angle (curvature) have been obtained for the first 20 modes of each of these panels, and the following observations have been made: (i) the majority of the low frequency modes are virtually independent of shell curvature; and (ii) the modes that are heavily influenced by curvature effects involve motion that is confined to the lengthwise edge regions of the panel.

1. INTRODUCTION

The vibration characteristics of completely free, open, cylindrically curved shell panels have received scant attention in the classical literature, because, like most other problems with unrestrained edges, no exact analytical solution is available. Resort has to be made to approximate solutions, and the earliest of these that (indirectly) addressed the title problem can be traced to Gontkevitch [1, 2]. He derived frequency determinants for open shells using the Ritz method with the assumed displacement field based on products of conventional beam functions and curved-beam functions; however, no explicit numerical results were reported. This work remained the only extant literature source on the title problem that Leissa [3] was able to reference in his comprehensive monograph of 1973. It was not until 1984 that Leissa and Narita [4] provided the first known set of comprehensive results for a completely free *shallow* shell, by using the Ritz method with polynomial assumed displacement functions. In a sequel published two years later [5], Narita and Leissa solved the same problem, but now with the shape of the platform boundaries generalized to accommodate curvilinear, rather than rectangular, edges. Subsequent literature searches [6] failed to reveal any further work on this particular topic prior to 1992; however, a number of relevant articles by Liew and Lim [7–10] have recently appeared in the literature devoted to the vibration of shallow shells. None of these papers contains results for freely suspended cylindrical shell panels, although it is clear from the

†Westland Lecturer in Helicopter Engineering.

0022–460X/97/450647 + 23 $25.00/0/sv971115

methodology employed by these authors that their *pb*-2 Ritz methodology would be capable of analyzing such problems. Notwithstanding this, it can be concluded that the completely free edge condition still remains one of the few largely unreported cases of the 18 496 [3] distinctly different panel boundary conditions that can exist for this problem; further study is clearly desirable.

In all the preceding work, with the exception of Gonkevitch's, the shell panels were assumed to be shallow, and the resulting analyses were based on a simplified set of shell equations [4]. In what follows, no such restrictions are made, and it is possible to model an arbitarily deep panel of constant curvature by using Love's full shell equations [11] with the modification introduced by Arnold and Warburton [12]. (A full discussion concerning the comparative merits and demerits of using shallow and deep shell theories has been presented by Lim, Kitipornchai and Liew [10].)

The layout of this paper naturally divides into two major sections. In the first part, the theoretical model is developed, and some convergence tests are conducted against the Leissa and Narita results [4]. In the second part, results are presented for three thin shells with aspect ratios (a/b) of 0·5, 1 and 2, the curvatures of which are gradually increased from nothing (i.e., a flat plate) until a complete—although unconnected—cylinder is obtained. Plots are presented of modal frequency versus included angle over the range $0^\circ \leqslant \phi \leqslant 360^\circ$, which clearly show the effect curvature has on the frequencies and modes of these panels. Some discussion, related to various features of the plots just mentioned, is given regarding the underlying physics of the problem.

The twofold purpose of this paper is, therefore, to provide a solution of the title problem and to provide some useful benchmark results for those engaged either in the dynamic analysis of restrained cylindrical shell panels, where it is customary to solve the completely free (unrestrained) problem first in order to check that the eigensolver is returning the correct number of zero frequency rigid body modes, or those engaged in experimental work, for which completely free edge conditions are the easiest to simulate in the laboratory.

2. METHOD OF ANALYSIS

An *h*-*p* version of the finite element method is utilized in what follows, because it affords the user a robust, flexible, and economic analysis tool that can accommodate geometric and material irregularities with greater facility than a conventional Ritz type of formulation. (If no such irregularities are present, which is the case for the title problem, then it can be shown that a single super-element with a high *p*-boost—which is effectively a Rayleigh–Ritz method—provides the most efficient solution, a finding which concurs with the work of other investigators [7, 9].)

The *h*-*p* method may be regarded as the marriage of the conventional *h*-version and *p*-version, in which convergence is now sought by simultaneously refining the mesh and increasing the degree of the elements [13–16]. For the type of problem under consideration here, in which the motions in all three co-ordinate directions are coupled, it is advantageous to represent both the out-of-plane displacements and the in-plane displacements by the *same* set of assumed modes. There are two good reasons for doing this: (i) it greatly reduces the computational effort required to calculate the element stiffness and mass matrices; and (ii) it simplifies the element assembly process.

An ascending hierarchy of *K*-orthogonal polynomials, used in conjunction with Hermite cubics, will furnish a complete set of admissible displacement functions with full C_1 continuity—that is, one that is capable of satisfying both displacement and slope continuity, in all three co-ordinate directions, across an element boundary (this set is

TABLE 1

The first ten C_1 shape functions used in this work

Hermite cubic shape functions	
	$f_1(\xi) = 1/2 - 3/4\xi + 1/4\xi^3$
	$f_2(\xi) = (1/8 - 1/8\xi - 1/8\xi^2 + 1/8\xi^3)L_E$
	$f_3(\xi) = 1/2 + 3/4\xi - 1/4\xi^3$
	$f_4(\xi) = (-1/8 - 1/8\xi + 1/8\xi^2 + 1/8\xi^3)L_E$
K-orthogonal polynomial shape functions	
	$f_5(\xi) = 1/8 - 1/4\xi^2 + 1/8\xi^4$
	$f_6(\xi) = 1/8\xi - 1/4\xi^3 + 1/8\xi^5$
	$f_7(\xi) = -1/48 + 3/16\xi^2 - 5/16\xi^4 + 7/48\xi^6$
	$f_8(\xi) = -1/16\xi + 5/16\xi^3 - 7/16\xi^5 + 3/16\xi^7$
	$f_9(\xi) = 1/128 - 5/32\xi^2 + 35/64\xi^4 - 21/32\xi^6 + 33/128\xi^8$
	$f_{10}(\xi) = 5/128\xi - 35/96\xi^3 + 63/64\xi^5 - 33/32\xi^7 + 143/384\xi^9$

summarized in Table 1). The Hermite cubics are used to define the displacements and rotations at the four nodes, and the hierarchical functions are used to provide additional degrees of freedom to the edges and interior of the element. (It is noted that an in-plane rotation can be regarded as a drilling degree of freedom, and as such represents an in-plane shear strain—rather than a displacement—at a node.) The nodal displacements/rotations and the amplitudes of the hierarchical functions along the edges and in the interior of the panel element constitute the generalized co-ordinates of the problem. Interelement compatibility is achieved simply by matching the generalized co-ordinates at common element nodes and along common edges.

Consider a thin, cylindrically curved, shell element, of uniform thickness h, bounded along its edges by the lines $x = 0$, $x = a$, $y = 0$ and $y = b$. (See Figure 1). Upon introducing the element-local non-dimensional co-ordinates ξ, η which are related to the element Cartesian co-ordinates through $\xi = 2x/a - 1$ and $\eta = 2y/b - 1$, the strain energy of the panel [11, 12] is given by

$$U = \frac{1}{2}\int_{-1}^{+1}\int_{-1}^{+1}\int_{-h/2}^{+h/2} \{\boldsymbol{\varepsilon}\}^{\mathrm{T}}\{\boldsymbol{\sigma}\}\,\frac{ab}{4}\,\mathrm{d}\eta\,\mathrm{d}\xi, \tag{1}$$

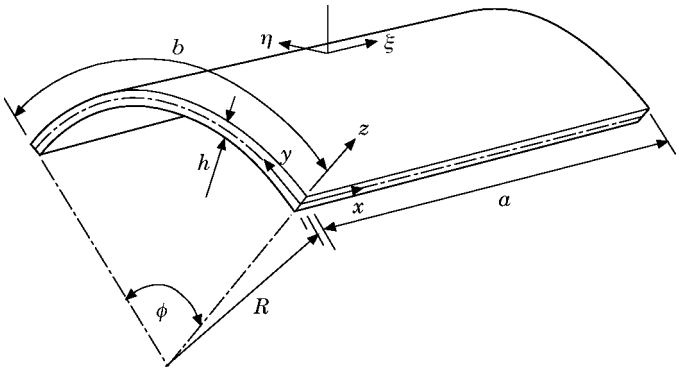

Figure 1. The curved panel element.

where the strain components are

$$\begin{bmatrix} \varepsilon_x \\ \varepsilon_y \\ \gamma_{xy} \end{bmatrix} = \begin{bmatrix} \frac{2}{a}\frac{\partial}{\partial\xi} & 0 & -z\frac{4}{a^2}\frac{\partial^2}{\partial\xi^2} \\ 0 & \frac{2}{b}\left(1-\frac{z}{R}\right)\frac{\partial}{\partial\eta} & -\frac{1}{R}-z\frac{4}{b^2}\frac{\partial^2}{\partial\eta^2} \\ \frac{2}{b}\frac{\partial}{\partial\eta} & \frac{2}{a}\left(1-2\frac{z}{R}\right)\frac{\partial}{\partial\xi} & -z\frac{8}{ab}\frac{\partial^2}{\partial\xi\,\partial\eta} \end{bmatrix} \begin{bmatrix} u(\xi,\eta) \\ v(\xi,\eta) \\ w(\xi,\eta) \end{bmatrix},$$

$$\text{i.e., } \{\boldsymbol{\varepsilon}\} = [\boldsymbol{\Delta}]\{\boldsymbol{\delta}\}, \tag{2}$$

and the material constitutive relationship is given by

$$\begin{bmatrix} \sigma_x \\ \sigma_y \\ \tau_{xy} \end{bmatrix} = \frac{E}{(1-\nu^2)} \begin{bmatrix} 1 & \nu & 0 \\ \nu & 1 & 0 \\ 0 & 0 & \frac{(1-\nu)}{2} \end{bmatrix} \begin{bmatrix} \varepsilon_x \\ \varepsilon_y \\ \gamma_{xy} \end{bmatrix}, \qquad \text{i.e., } \{\boldsymbol{\sigma}\} = [\mathbf{D}]\{\boldsymbol{\varepsilon}\}. \tag{3}$$

Both the in-plane displacement fields u and v, and the out-of-plane displacement field w, may approximately be represented by a finite series of the previously assumed modes in the ξ- and η-directions; namely,

$$u(\xi,\eta) = \sum_{rx=1}^{p_{ux}} \sum_{sx=1}^{p_{uy}} X_{rx,sx} f_{rx}(\xi) f_{sx}(\eta), \qquad v(\xi,\eta) = \sum_{ry=1}^{p_{vx}} \sum_{sy=1}^{p_{vy}} Y_{ry,sy} f_{ry}(\xi) f_{sy}(\eta), \tag{4a, b}$$

and

$$w(\xi,\eta) = \sum_{rz=1}^{p_{wx}} \sum_{sz=1}^{p_{wy}} Z_{rz,sz} f_{rz}(\xi) f_{sz}(\eta). \tag{4c}$$

$X_{rx,sx}$, $Y_{ry,sy}$ and $Z_{rz,sz}$ are the [unknown] generalized co-ordinates of the problem, and each summation is taken over (any number of) p assumed modes. (The first subscript on p denotes the type of displacement field; the second denotes whether it is in the x- or y-direction.)

Equation (4) can be written more succinctly in matrix notation as

$$\{\boldsymbol{\delta}\} = [\mathbf{N}]\{\mathbf{q}\}, \tag{5}$$

where $\boldsymbol{\delta} = \{u(\xi,\eta),\ v(\xi,\eta),\ w(\xi,\eta)\}^{\mathrm{T}}$, $\mathbf{q} = \{X_{rx,sx}, Y_{ry,sy}, Z_{rz,sz}\}^{\mathrm{T}}$ and $\mathbf{N}$ is a rectangular matrix containing the shape functions. Hence, substituting equations (2, 3, 5) into equation (1) yields

$$\mathbf{U} = \tfrac{1}{2}\{\mathbf{q}\}^{\mathrm{T}}\left[\frac{ab}{4}\int_{-1}^{+1}\int_{-1}^{+1}\int_{-h/2}^{+h/2} ([\boldsymbol{\Delta}][\mathbf{N}])^{\mathrm{T}}[\mathbf{D}][\boldsymbol{\Delta}][\mathbf{N}]\,\mathrm{d}\eta\,\mathrm{d}\xi\,\mathrm{d}z\right]\{\mathbf{q}\}. \tag{6}$$

The term in the square brackets is clearly the plate element stiffness matrix $\mathbf{K}^{\mathrm{E}}$.

Likewise, in element-local co-ordinates, the kinetic energy of the plate is given by

$$T = \tfrac{1}{2}\rho\int_{-1}^{+1}\int_{-1}^{+1}\int_{-h/2}^{+h/2} \{\dot{\boldsymbol{\delta}}\}^{\mathrm{T}}\{\dot{\boldsymbol{\delta}}\}\frac{ab}{4}\,\mathrm{d}\eta\,\mathrm{d}\xi\,\mathrm{d}z. \tag{7}$$

Substituting equation (5) into equation (7) yields

$$T = \tfrac{1}{2}\{\dot{\mathbf{q}}\}\left[\rho\,\frac{ab}{4}\int_{-1}^{+1}\int_{-1}^{+1}\int_{-h/2}^{+h/2}[\mathbf{N}]^{\mathrm{T}}[\mathbf{N}]\,\mathrm{d}\eta\,\mathrm{d}\xi\,\mathrm{d}z\right]\{\dot{\mathbf{q}}\}. \tag{8}$$

Evidently, the term in the square brackets is the plate element mass matrix $\mathbf{M}^E$.

Both $\mathbf{K}^E$ and $\mathbf{M}^E$ are comprised of nine sub-matrices; namely, one direct bending, two direct stretching, four coupled bending–stretching and two coupled stretching–stretching. Equation (4) gives the overall order as $(p_{ux} \times p_{uy}) + (p_{vx} \times p_{vy}) + (p_{wx} \times p_{wy})$.

The matrix multiplication and integration required to evaluate the element stiffness and mass matrices shown in equations (6) and (8) was performed symbolically (for a maximum of ten assumed in-plane and out-of-plane modes in both the x- and y-directions) by using the computer algebra package MAPLE [17]. This enables all the entries in $\mathbf{K}^E$ and $\mathbf{M}^E$ to be determined in exact, fractional, algebraic format, and then downloaded to the main analysis program where they are stored at a familial level. In this way, no numerical rounding errors are introduced in the calculation of the element stiffness and mass matrices; also, only one significant computational expense is ever incurred, because, by keeping $\mathbf{K}^E$ and $\mathbf{M}^E$ completely generic, the integration has only to be performed once.

The h-p method of assembling the elements to obtain the global stiffness and mass matrices is slightly different from the standard h-version technique, on account of the internal polynomial enrichment that is available in each element. The formulation of the element stiffness and mass matrices is in accordance with the theory espoused previously, with each entry in the matrix corresponding to a particular generalized co-ordinate. The first stage in formulating an assembly process is to re-order these matrices such that the generalized co-ordinates $\mathbf{q}$ appear in the following sequence: nodal (i.e., corner), edge and purely internal; this is illustrated schematically by

$$\mathbf{K}^{\mathrm{E}} \text{ or } \mathbf{M}^{\mathrm{E}} = \begin{bmatrix} [N.N] & [N.E.] & [N.I] \\ [E.N] & [E.E] & [E.I] \\ [I.N] & [I.E] & [I.I] \end{bmatrix}. \tag{9}$$

There are always the following: 16 w-wise, eight u-wise and eight v-wise nodal degrees of freedom ($\equiv N$ in the notation of equation (9), which correspond to the use of the four Hermite cubics; $4(p_{wx}-4)+4(p_{wy}-4)$ w-wise, $4(p_{uy}-4)+8+2(p_{ux}-4)$ u-wise and $4(p_{vx}-4)+8+2(p_{vy}-4)$ v-wise edge degrees of freedom ($\equiv E$ in the notation of equation (9)), which correspond to the products of the Hermite cubics with the hierarchical modes; $(p_{wx}-4)(p_{wy}-4)$ w-wise, $2(p_{ux}-4)+(p_{ux}-4)(p_{uy}-4)$ u-wise and $2(p_{vy}-4)+(p_{vx}-4)(p_{vy}-4)$ v-wise purely internal degrees of freedom ($\equiv I$ in the notation of equation (9)), which correspond to the products of only the hierarchical modes.

It is now possible to form the global stiffness and mass matrices, by identifying, and then adding together, all the like terms from any number of adjacent elements which correspond to common nodal and edge degrees of freedom along their interface. Note the following: (i) the purely internal modes from one element cannot "affect" the purely internal modes from any other element, and so these contributions to the global stiffness and mass matrices remain unaffected by the assembly process—in fact, $[I.I]^{\mathrm{G}}$ will be block diagonal; (ii) all edge-to-edge interfaces are fully conforming; and (iii) since the in-plane motion in the shell (or plate) is governed by two, coupled, *second* order differential equations, it is only necessary to match the *displacements* u and v across an element interface to ensure C_0 continuity; *first derivative* continuity (i.e., $\partial u/\partial\eta$, $\partial v/\partial\eta$, $\partial u/\partial\xi$ and $\partial v/\partial\xi$, which effectively describes the in-plane shear and direct strain/stress at a point)

across the interface will approximately be satisfied as a consequence of the energy method used.

The final structure of $\mathbf{K}^G$ and $\mathbf{M}^G$ is similar to the partitioned format shown in equation (9), except that now the dimensions of the sub-matrices are significantly larger than, and their content significantly different from, those for an individual element.

Although a variety of different boundary conditions may be applied to the panel by nullifying the appropriate generalized co-ordinates, it is not necessary to do this in the current work, and $\mathbf{K}^G$ and $\mathbf{M}^G$ remain completely intact.

By assuming simple harmonic motion and the absence of any external forcing agency, the governing equations of motion can be derived by substituting the total potential energy expression into Lagrange's equation. This yields a standard matrix-eigenvalue problem of the form

$$[[\mathbf{K}] - \Omega^2[\mathbf{M}]]\{\mathbf{q}\} = 0, \tag{10}$$

where the non-dimensional frequency is rendered not in terms of the usual shell ring frequency but rather in terms of a flat plate frequency $\Omega^2 = \rho h\omega^2 b^4/D$, where D is the flexural rigidity of the panel $Eh^3/12(1 - \nu^2)$. The reason for choosing this frequency measure is two-fold: (i) it permits a direct comparison to be made with the work on shallow shells reported by other investigators; and (ii) it is the best way of quantifying the effect on the *radian* (dimensional) frequency of varying parameters such as the panel's radius of curvature. The solution of equation (10) yields the natural frequencies. The first six of these are always zero, corresponding to rigid-body modes; these will be disregarded in the "numbering" of the elastic modes. Corresponding to each eigenvalue is an eigenvector, which may be used in conjunction with equation (4) to recover the associated displacement of each element in the model, and hence the complete mode of the panel under consideration.

3. CONVERGENCE STUDY

A convergence study was undertaken using three different h meshes, each with different amounts of p-enrichment, for a completely free, square planform, shallow shell with the following geometry: $a/h = 100$, $a/b = 1{\cdot}01$, the included angle $\phi = 28{\cdot}96^\circ$, and Poisson ratio $\nu = 0{\cdot}3$. The reason such unusual parameters have been chosen is simply to enable a strict, like-for-like comparison to be conducted against the work of Leissa and Narita [4]*; in this manner, their results can be used as a benchmark solution for the present method. The frequencies of the first four elastic modes are presented in Table 2. As would be expected, the frequency parameters are seen to converge monotonically from above, yielding upper bounds to the exact values. The four- and eight-element meshes provide marginally more accurate results than the single super-element, as would be expected, albeit at a vastly inflated "cost" considering the number of degrees of freedom (dof) involved. However, it is worth noting that for a *given* number of degrees of freedom, the solution arising from the use of a single super-element mesh is always the more accurate. Independent verification has been obtained from a standard finite element analysis using the proprietary package ANSYS [18]. The frequency results arising from different meshes constructed from the four-noded SHELL-63 element are included in Table 2 for completeness. The results from both the h-p methodology and ANSYS agree to a remarkable degree; however, some differences are noticed between these sets of results and those of Leissa and Narita. There are two likely sources of error that can account for

* Leissa and Narita defined the aspect ratio a/b in terms of the *projected* length of the curved edge, rather than the actual length of the curved edge adopted here.

TABLE 2

Convergence study based on three different mesh designs: the first four non-dimensional frequencies of a completely free cylindrical shell ($a/h = 100$, $a/b = 1{\cdot}01$, $\phi = 28{\cdot}95^\circ$ *and* $\nu = 0{\cdot}3$)

	Current method	Ω_1	Ω_2	Ω_3	Ω_4	dof
$h = 1$	$p = 6$	13.423	21.678	34.709	49.815	108
	$p = 8$	13.403	21.475	34.148	48.917	192
	$p = 10$	13.403	21.473	34.147	48.908	300
$h = 4$	$p = 6$	13.403	21.475	34.151	48.926	320
	$p = 8$	13.403	21.473	34.147	48.907	616
	$p = 10$	13.403	21.473	34.147	48.906	1 008
$h = 8$	$p = 6$	13.403	21.474	34.148	48.910	588
	$p = 8$	13.403	21.473	34.147	48.907	1 160
	$p = 10$	13.403	21.473	34.147	48.906	1 924
ANSYS 30×30		13.407	21.476	34.165	48.963	5 766
ANSYS 50×50		13.404	21.474	34.153	48.926	15 606
ANSYS 100×100		13.403	21.473	34.148	48.913	61 206
Leissa and Narita [4]		13.508	22.073	34.868	48.703	75

this difference: (i) the different types of shell theory employed: and (ii) the acknowledged level of (incomplete) convergence in Leissa and Narita's work. However, sufficient agreement has been demonstrated to inspire confidence in the current methodology.

4. RESULTS

Rather than present a series of *ad hoc* results for arbitrary panel geometries, it was decided that a more effective strategy would be to fix the panel planform and thickness, and then vary the radius of curvature such that a flat plate is realized at one extreme, and a full, although unjoined, cylinder is obtained at the other. By taking panel aspect ratios a/b of 0·5, 1 and 2, and fixing the shell thickness* $h = b/2000$ and Poisson ratio $\nu = 0{\cdot}3$, a large range and combination of geometric parameters can be studied without rendering this article unduly prolix.

In Figures 2, 3 and 4 are presented plots of frequency versus included angle for the first 20 elastic modes of the aformentioned panels with aspect ratios a/b of 0·5, 1 and 2 respectively. All of these results have been generated using a fixed mesh design comprising four elements around the shell circumference; the levels of p-enrichment in the η- and ξ-directions were eight and ten respectively, for all three components of displacement, within each element. This level of mesh refinement—which amounts to an 810 dof problem—ensured the results for the first 20 modes (2·5% of the total number yielded) were fully converged. A logarithmic scale was chosen for the abscissa (included angle ϕ) simply because the most complicated modal behaviour takes place within the first 10°, and it was felt important to show this clearly.

* For all three shells, the length of the curved edge, b, is fixed, and the length of the straight edge, a, is varied to give the appropriate aspect ratio. Hence b is used as the basis for the non-dimensional frequency factor in equation (10), and the non-dimensional thickness-to-length ratio. The latter value of $h/b = 1/2000$ has been used simply to preserve the *thin* shell criterion.

On each figure, the shell ring frequency $\omega_R = (E/\rho)^{1/2}/R$, which becomes $\Omega_R = \phi(b/h)\,[12(1-\nu^2)]^{1/2}$ on the plate non-dimensional frequency scale, is plotted as a dashed line. It is evident from each figure, but especially so on Figure 2 ($a/b = 0{\cdot}5$) that, for a given shell, the modal density (number of modes per unit frequency) increases significantly in the region of the ring frequency, which accords with expectation [19].

In order to quantify further the vibrational behaviour of these panels, the first 12 elastic modes of the square planform shell with included angles of 0°, 1°, 10°, 100° and 360° are presented in Figures 5, 6, 7, 8 and 9 respectively. The modes for the other two rectangular panels exhibit most, if not all, of the features observed for the square panel, and do not therefore warrant inclusion here.

It should be noted that the lengthwise edges of the full, unjoined, cylinder can theoretically overlap on part of their cycle, as typified by case Ω_3 in Figure 9. The results are not intended to suggest such a "slit tube" would constitute a viable structure—rather, they complete the set of results presented here, and provide a stark contrast to the modes that would exist in a freely suspended *closed* cylindrical tube.

4.1. GENERAL OBSERVATIONS

When the radius of curvature is infinite (corresponding to zero included angle), the frequencies of a completely free flat plate are obtained. (Note, however, that it is not possible to show these when using logarithmic axes.) It is well-known [20] that for plates

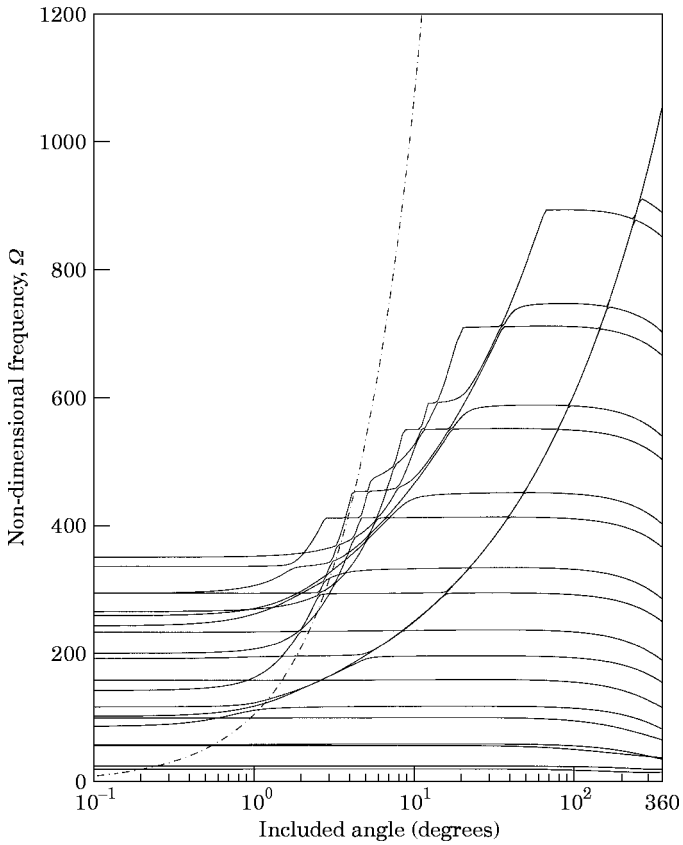

Figure 2. Frequency variation as a function of included angle of curvature for the first 20 modes of a curved panel ($a/b = 0{\cdot}5$, $b/h = 2000$ and $\nu = 0{\cdot}3$).

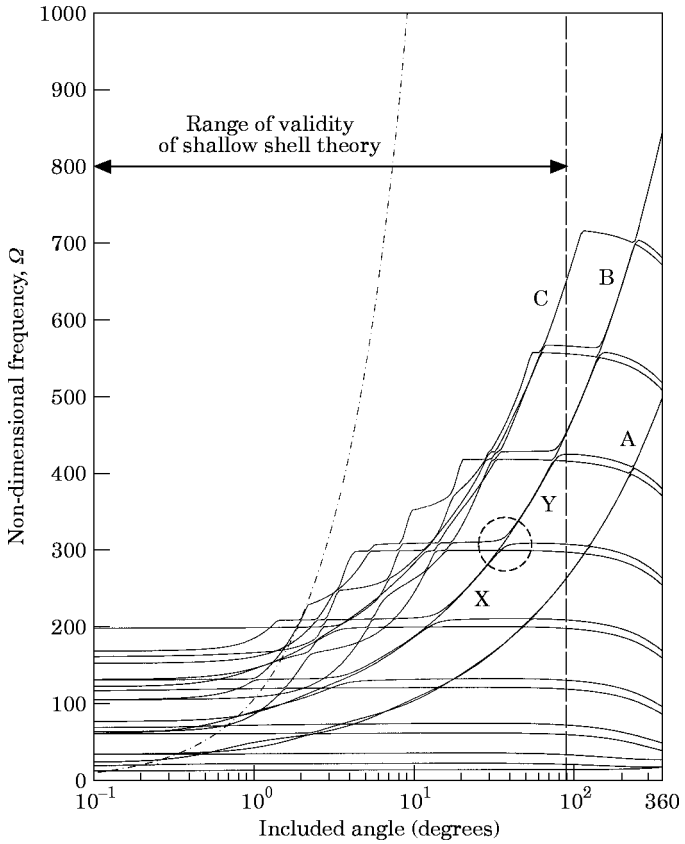

Figure 3. Frequency variation as a function of included angle of curvature for the first 20 modes of a curved panel ($a/b = 1{\cdot}0$, $b/h = 2000$ and $\nu = 0{\cdot}3$).

with certain aspect ratios, some of their modes are degenerate. For example, a completely free square plate will have the following (elastic) degenerate pairs: modes 4 and 5 at $\Omega = 34{\cdot}801$, modes 6 and 7 at $\Omega = 61{\cdot}093$, modes 11 and 12 at $\Omega = 105{\cdot}461$, and modes 15 and 16 at $\Omega = 131{\cdot}472$. Reference to Figure 3 makes it clear that such degeneracies are destroyed for all $\phi > 0^\circ$; the apparent display of degenerate pairs up to $\phi = 0{\cdot}1^\circ$ arises as a consequence of the relatively large scale used on the frequency axis. The reason degenerate pairs separate upon the introduction of curvature is due to the now different flexural stiffnesses in the ξ- and η-directions—a curved shell is stiffer in a direction along its generator than in a direction around its circumference. This effectively renders the stiffness of the panel orthotropic, and hence degenerate modes for the square flat plate become distinctly different when the panel is curved slightly.

For all three shells considered here, the frequency of the fundamental mode, and some of the higher modes, is more or less independent of the amount of curvature. An explanation can be found by examining the first and second modes of vibration of the square panel shown in Figures 5–9, cases Ω_1 and Ω_2.

The first mode consists of a predominantly twisting action about the ξ- and η-axes, leading to an antisymmetric–antisymmetric mode of vibration. The torsional rigidity about either axis is unaffected by curvature, but the polar second moment of area (which dictates the mass inertia), and the separation between the centre of mass (bending) and the shear

centre (twisting), will change with increasing curvature. These latter effects affect the frequency of this mode only when the angle of curvature exceeds 100°.

For the range of angles shown in Figure 3, the second mode involves predominantly out-of-plane bending in the η-direction, with little or no in-plane extensional motion (middle surface stretching). (A contour plot taken at $z = 0$ would show nodal lines that are nearly parallel to the generator of the cylinder, becoming increasingly straight with increasing curvature.) Because I_η does not change with increasing curvature, the frequency again will remain constant as a function of curvature until elastic coupling effects between the in-plane and out-of-plane motions become significant. These findings are consistent with the results given by Leissa and Narita [4]. (It can be noted from Figure 5 that the second mode of the *flat* plate is distinctly different from, and occurs at a significantly lower frequency than, the results reported for panels with $\phi \geqslant 1°$. Again, this accords with the findings of Leissa and Narita [4].)

Also, the greater the value of a/b, the greater the tendency for the lower frequency modes to involve bending both around *and* along the length of the panel. For this reason, the first four modes of the $a/b = 0{\cdot}5$ panel consist only of bending motions around the shell circumference, whereas for the $a/b = 2$ panel, the corresponding four modes are interleaved with other modes involving bending in both directions.

It can be seen in Figures 2, 3 and 4 that a lot of complicated low frequency mode re-ordering takes place within the first 10° of included angle, after which a more settled

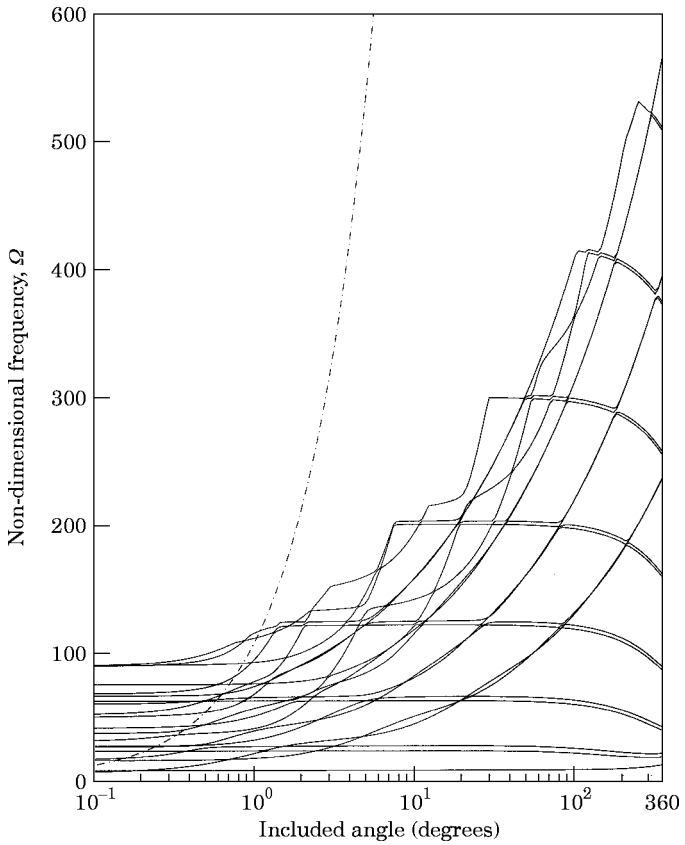

Figure 4. Frequency variation as a function of included angle of curvature for the first 20 modes of a curved panel ($a/b = 2{\cdot}0$, $b/h = 2000$ and $\nu = 0{\cdot}3$).

trend appears. For the square panel, this trend may best be described between $10^\circ \leqslant \phi \leqslant 90^\circ$ as a series of pairs of horizontal lines, traversed by (in this case) three steeply ascending curves (denoted A, B and C in Figure 3). For included angles in excess of 90°, a general reduction in the frequencies of all but the first three modes is apparent. (Although this latter range is somewhat compressed in Figures 2, 3 and 4 due to the use of a logarithmic scale, it nonetheless represents three-quarters of the included angle range considered here.) The observed reduction in frequency occurs beyond the previously quoted range of validity of shallow shell theory (this range has been indicated on Figure 3).

To conclude this general overview, it is interesing to note that the frequencies of some of the early modes—e.g., modes 7 and 8 of the $a/b = 2$ panel (see Figure 2)—can increase by as much as 50% when the panel is curved by some 5°. Hence investigators should be aware of the difficulties that may be experienced in obtaining consistent results with experimental work—any slight handling damage that introduces a minute amount of curvature would render useless any measurements taken on a supposedly flat plate. (Note that, for small angles, the ratio of the panel thickness to the mid-span rise above the horizontal can be shown to be $8h/b\phi$; for the current shell, with $h/b = 1/2000$ and 5° of included angle, this ratio equals 0·046. In other words, the mid-span rise is approximately 22 times the panel thickness, which, although small, *is* nonetheless a noticeable amount of curvature.)

4.2. SPECIFIC OBSERVATIONS FOR THE SQUARE PLANFORM PANEL

In the preceding section it was explained why the frequencies of the first two modes remained more or less independent of the amount of shell curvature. Likewise, the general trend of the modal frequency curves to the right of the ring frequency curve were described. However, it is worth considering this modal behaviour in greater detail, since there are some interesting manifestations that hitherto have not been reported. With the aid of Figures 5–9, it can be seen that the series of near horizontal pairs of lines shown in Figure 3 to the right of the ring frequency curve correspond to modes exhibiting increasing numbers of half-waves in the (η) circumferential direction, with near linear symmetric and antisymmetric displacements in the length-wise (ξ) direction.

For a given pair, the mode exhibiting symmetry about the η-axis always occurs at a lower frequency than its companion mode exhibiting asymmetry—that is, straight edge twisting—about the η-axis. A view directly on to the curved end of the panel would confirm that these modes are the panel equivalent of the free–free modes of a curved beam. To the left of the ring frequency, this dichotomous behaviour is less obvious, although it can still be identified, albeit in a less distinct fashion. The frequencies of this family of modes are largely independent of the amount of curvature present since they all involve bending around the circumference, with nodal lines parallel with a shell generator.

Perhaps of greater interest is the significance of the three steeply ascending curves (denoted A, B and C in Figure 3); actually there are two overlapping lines constituting each of these curves. Consider "curve" A: (almost) degenerate modes 10 and 11 occur at frequencies of $\Omega = 274{\cdot}314$ and 274·612 respectively for the 100° shell; closely spaced modes 6 and 7 occur at frequencies of $\Omega = 103{\cdot}053$ and 105·859 respectively for the 10° shell. From Figure 8 (cases Ω_{10} and Ω_{11}) and Figure 7 (cases Ω_6 and Ω_7) , it can be seen that these modes involve elastic motion which is restricted to the panel edges at $\eta = \pm 1$, with the rest of the shell remaining motionless. These panel "edge" modes always occur in symmetric/antisymmetric pairs about the ξ-axis, and exhibit one clear half wavelength of motion along the length. In effect, the lengthwise edges are behaving as uncoupled, high aspect ratio, cantilevered shell panels. "Curve" A thus describes the pair of fundamental panel "edge modes". It can also be seen from Figures 7 and 8 that increasing the curvature

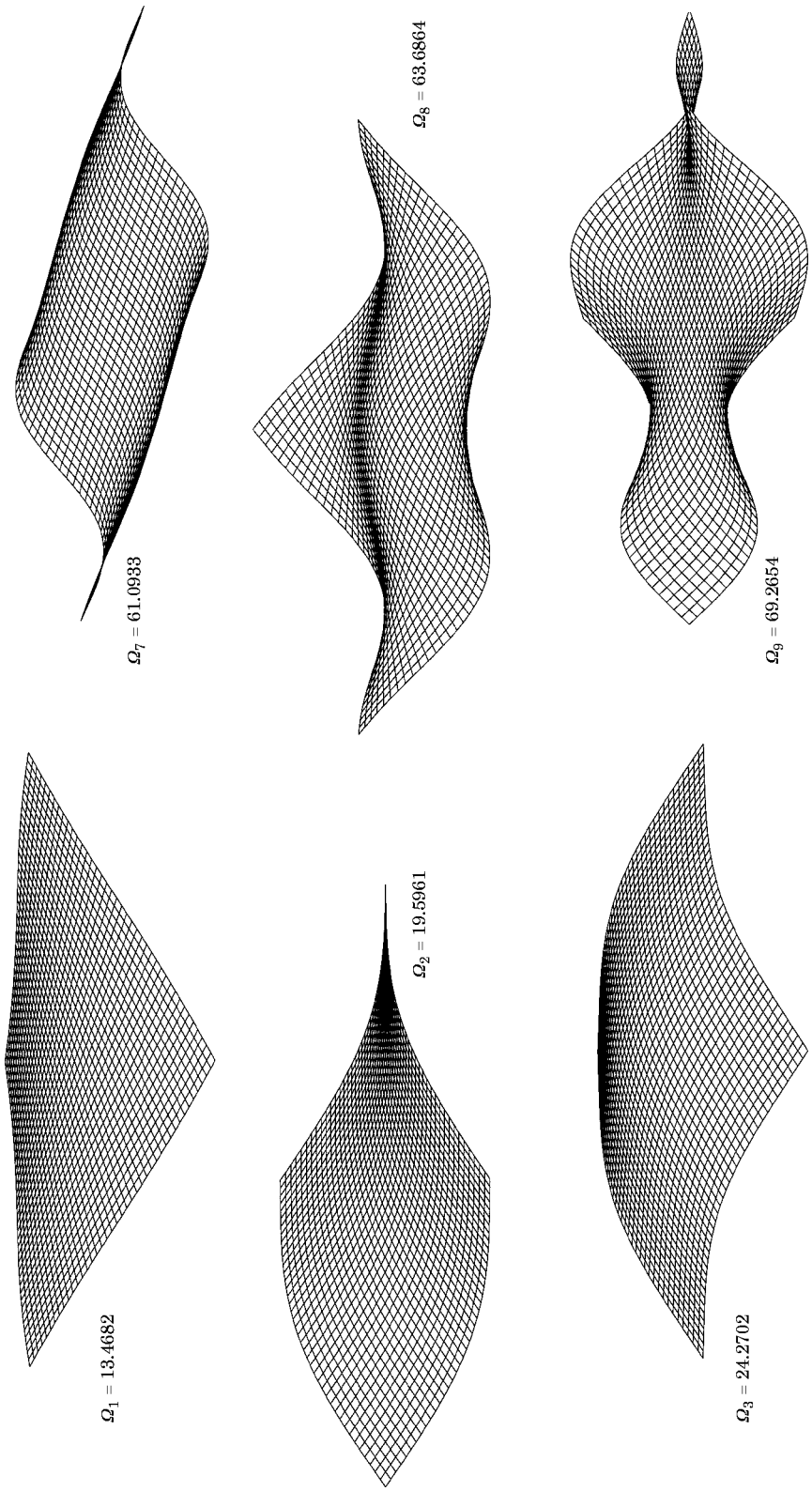
$\Omega_1 = 13.4682$
$\Omega_2 = 19.5961$
$\Omega_3 = 24.2702$
$\Omega_7 = 61.0933$
$\Omega_8 = 63.6864$
$\Omega_9 = 69.2654$

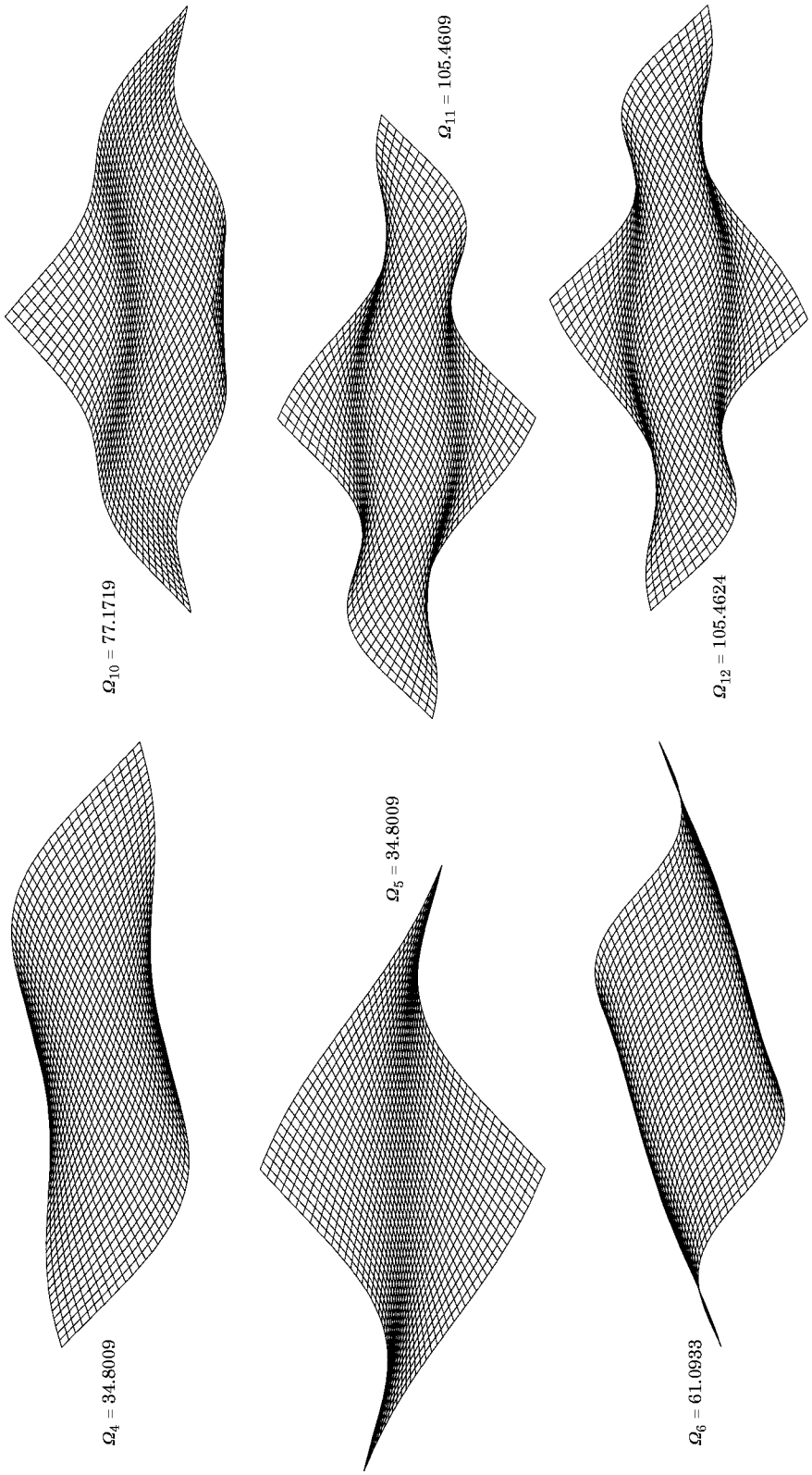

Figure 5. The first 12 modes of vibration of a square planform panel ($\phi = 0°$).

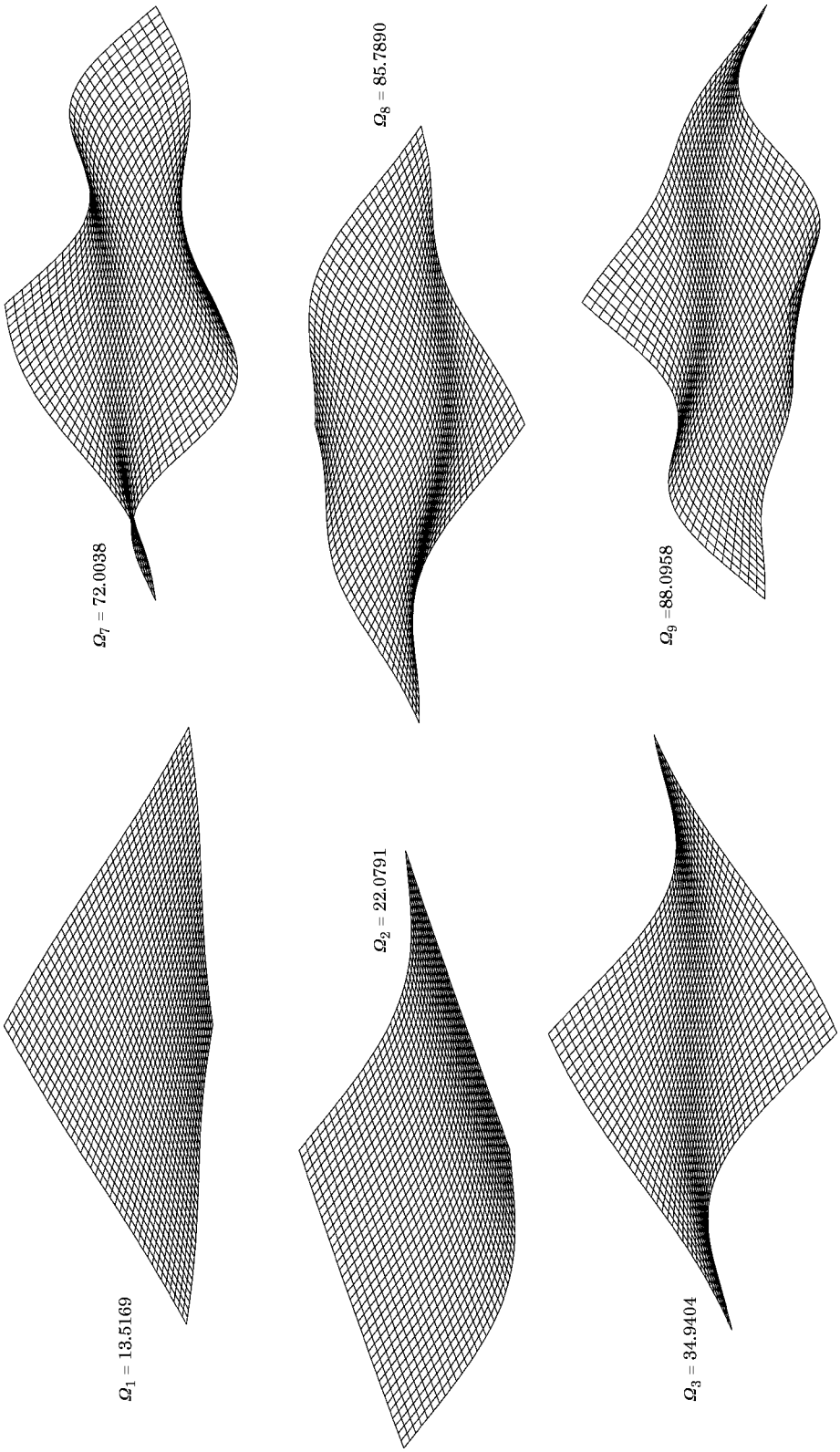
$\Omega_1 = 13.5169$
$\Omega_2 = 22.0791$
$\Omega_3 = 34.9404$
$\Omega_7 = 72.0038$
$\Omega_8 = 85.7890$
$\Omega_9 = 88.0958$

Figure 6. The first 12 modes of vibration of a square planform panel ($\phi = 1°$).

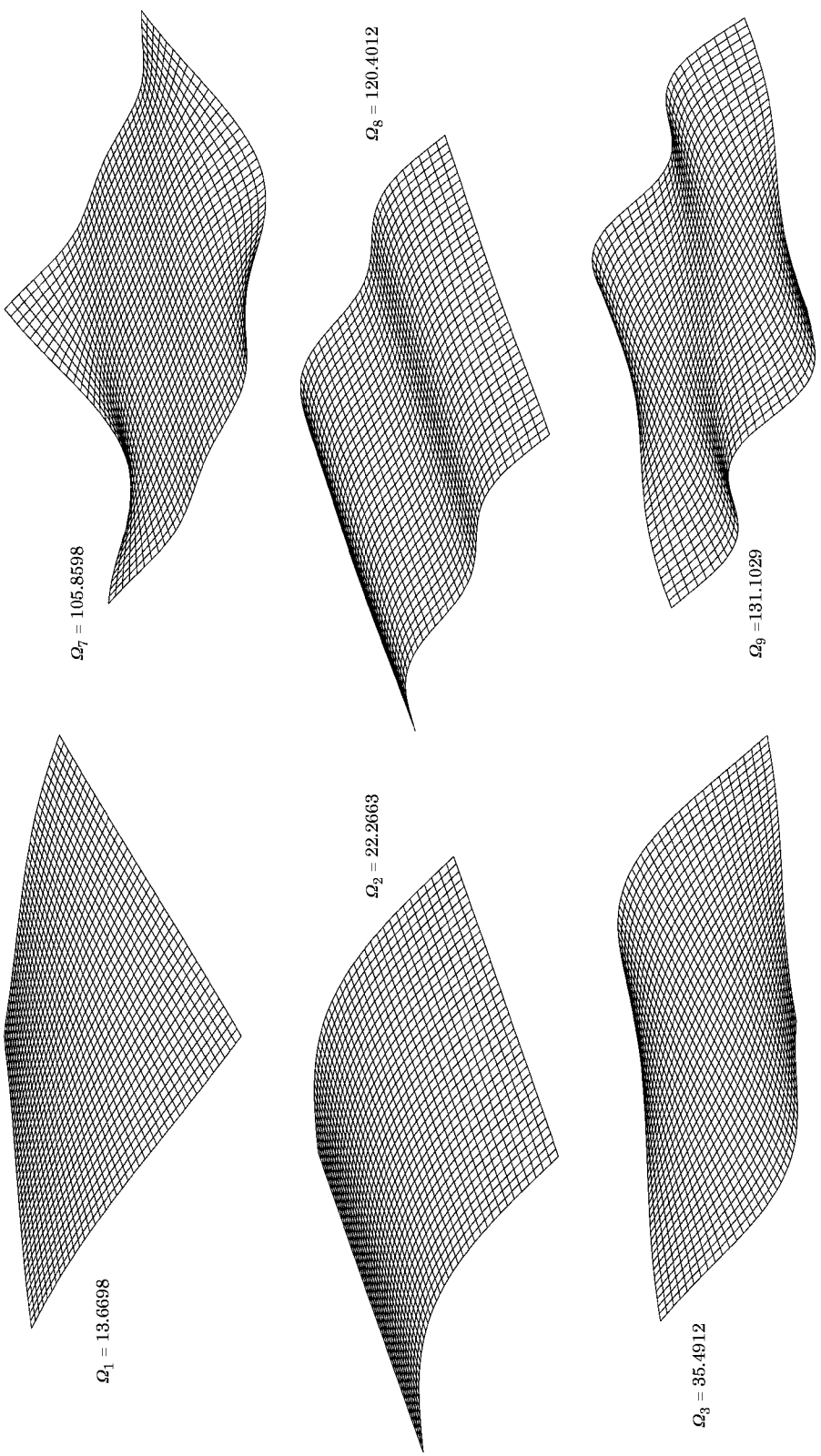
$\Omega_1 = 13.6698$
$\Omega_2 = 22.2663$
$\Omega_3 = 35.4912$
$\Omega_7 = 105.8598$
$\Omega_8 = 120.4012$
$\Omega_9 = 131.1029$

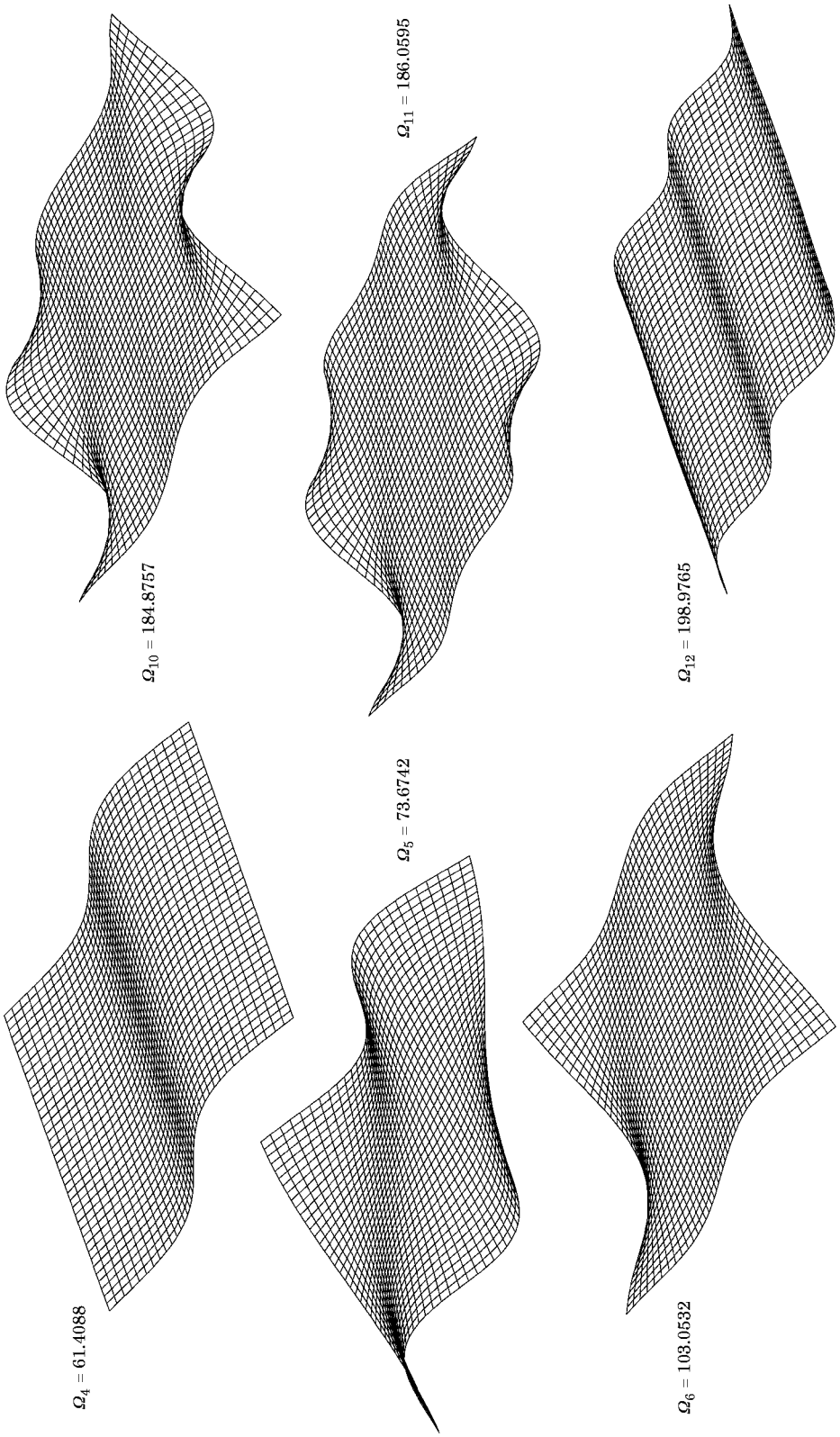

Figure 7. The first 12 modes of vibration of a square planform panel ($\phi = 10^\circ$).

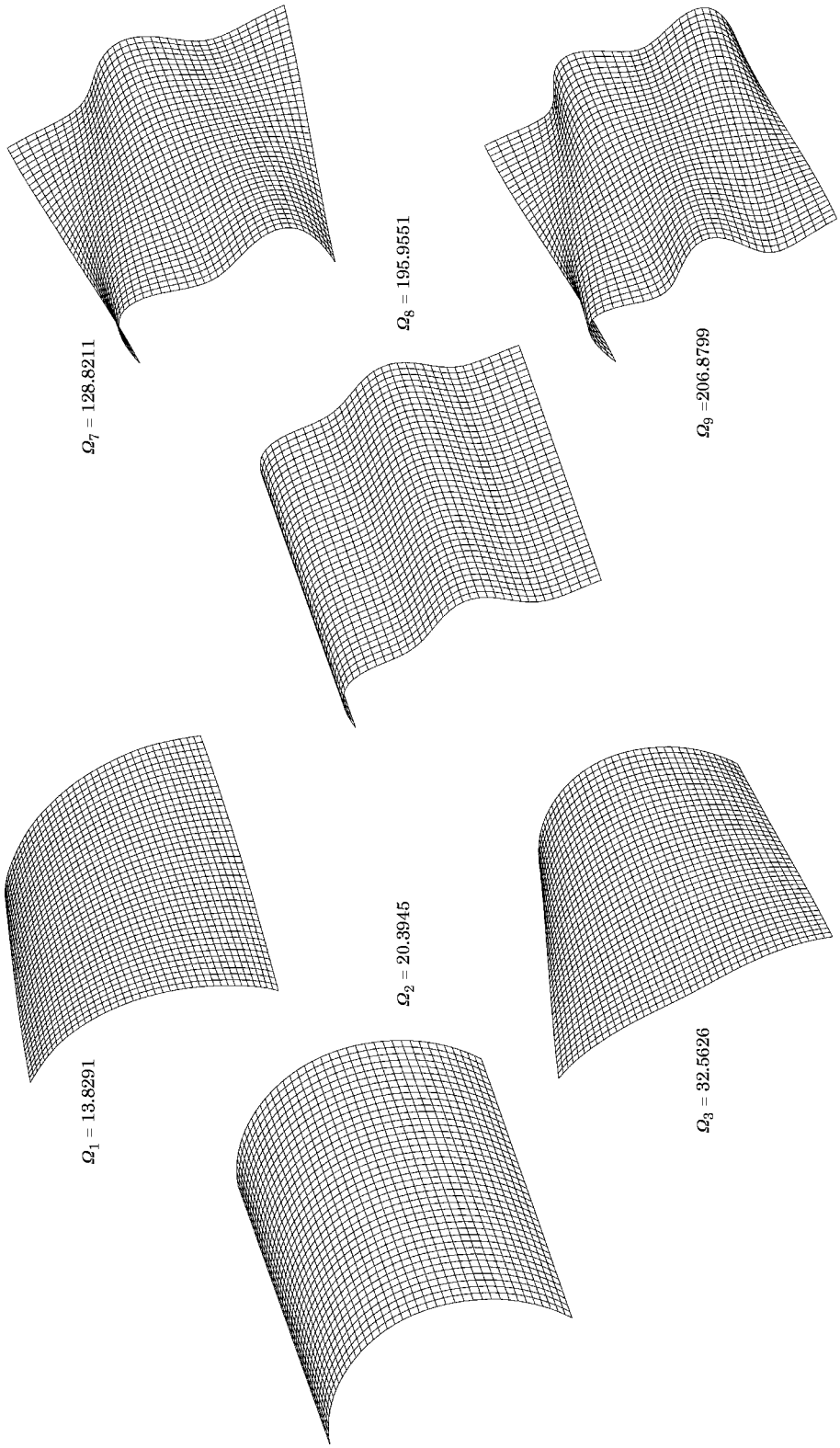
$\Omega_1 = 13.8291$
$\Omega_2 = 20.3945$
$\Omega_3 = 32.5626$
$\Omega_7 = 128.8211$
$\Omega_8 = 195.9551$
$\Omega_9 = 206.8799$

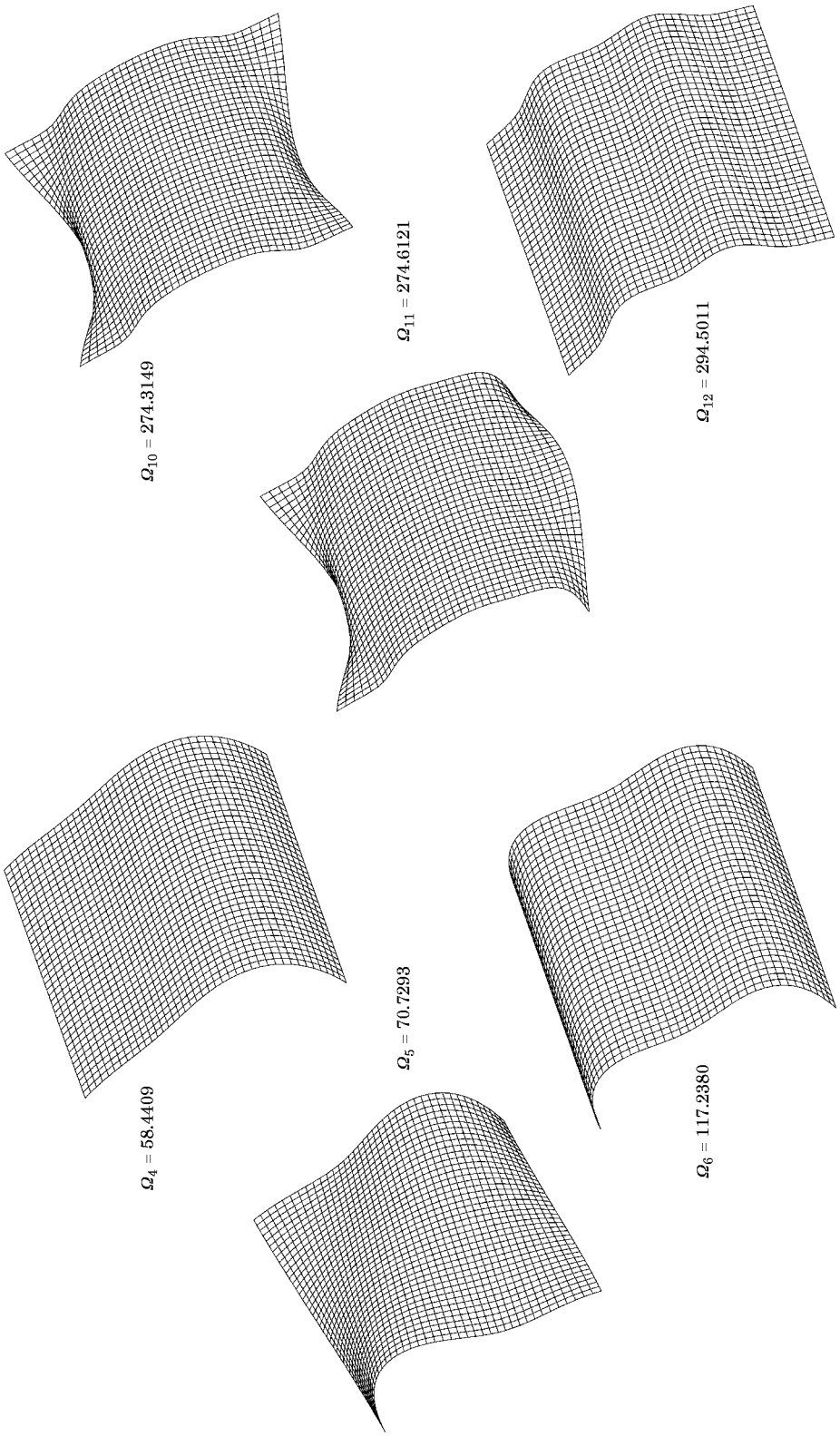

Figure 8. The first 12 modes of vibration of a square planform panel ($\phi = 100^\circ$).

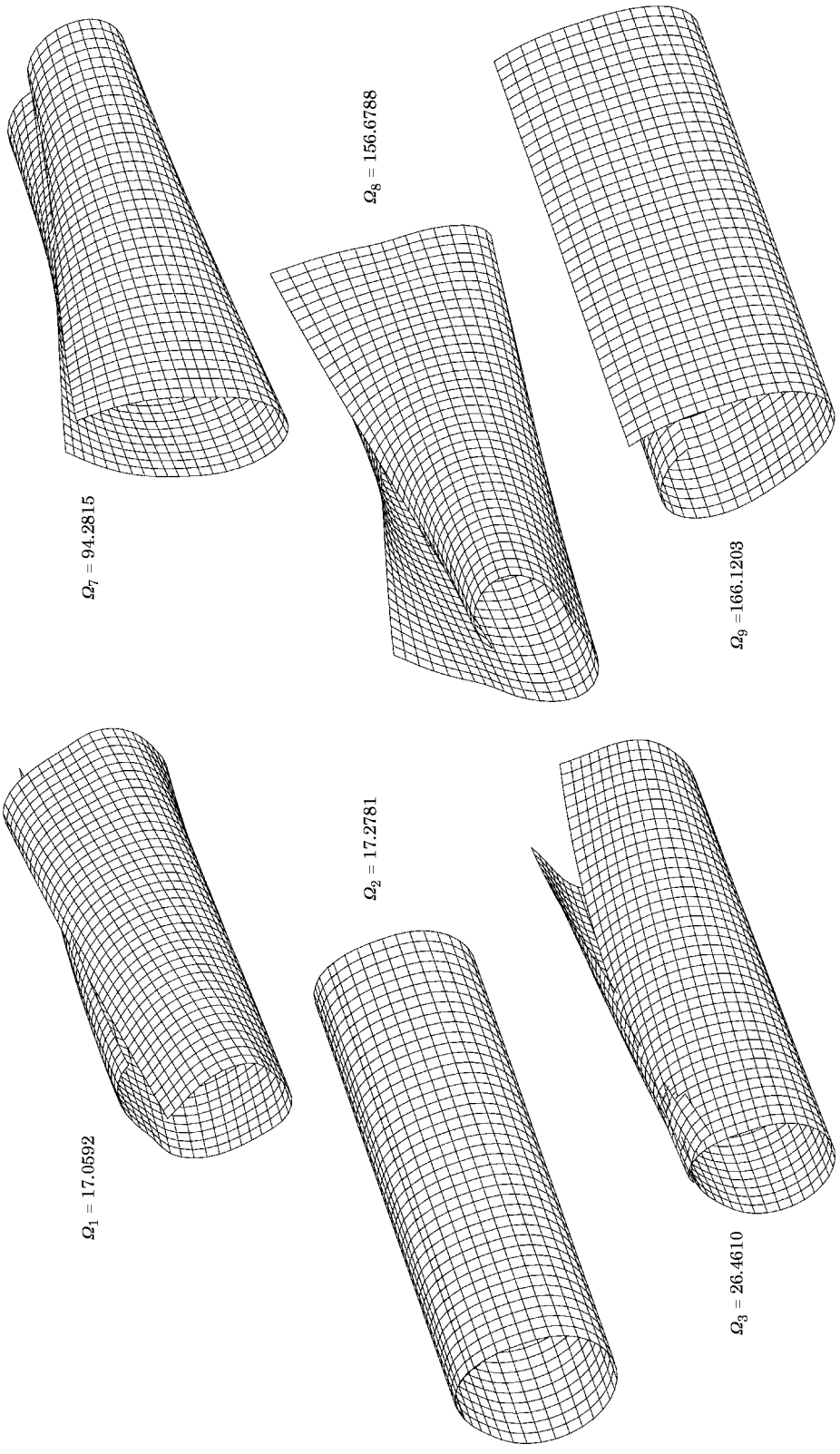
$\Omega_1 = 17.0592$
$\Omega_2 = 17.2781$
$\Omega_3 = 26.4610$
$\Omega_7 = 94.2815$
$\Omega_8 = 156.6788$
$\Omega_9 = 166.1203$

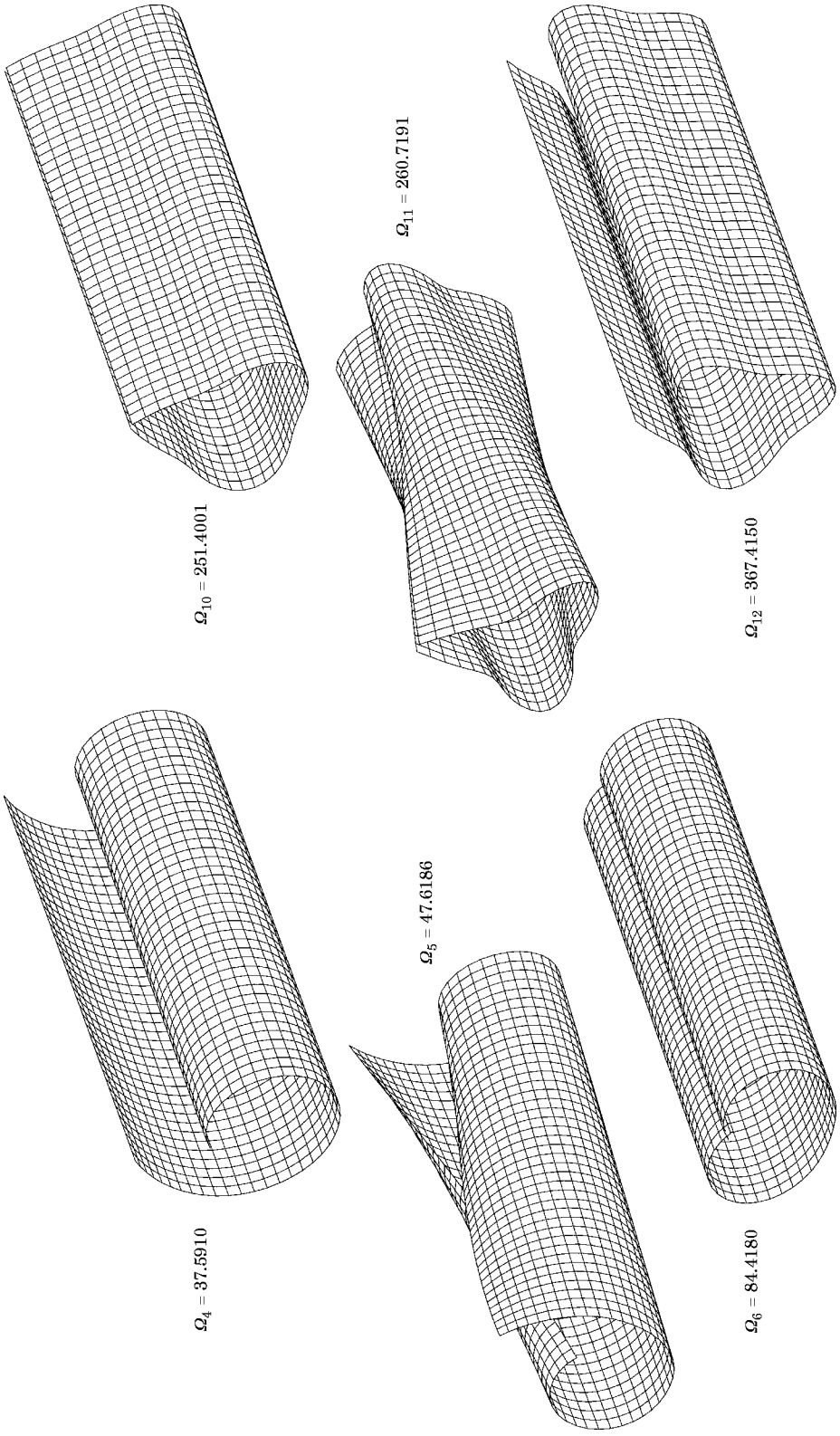

Figure 9. The first 12 modes of vibration of a square planform panel ($\phi = 360^\circ$).

of the panel decreases the width of the curved edge capable of motion and thus effectively raises the "aspect ratio" of the cantilevered shell edge and hence increases the frequency of its edge modes. (A similar effect has been noted by Lee, Leissa and Wang [21] concerning localized bending along the free edges of a cantilevered shell panel, suggesting this mechanism manifests itself in structures other than completely free ones.)

The first overtone of this pair of "edge modes" can be found on curve B in Figure 3, and visualized from modes 10 and 11 ($\Omega = 184{\cdot}875$ and $186{\cdot}059$) in Figure 7 (cases Ω_{10} and Ω_{11}) for the 10° shell. Two half-wavelengths now exist along both η-wise edges. Likewise, curve C describes the second overtone of the panel "edge modes" in this series, with three half-wavelengths along each edge, and so on.

Where an "edge mode" curve "crosses" a closely spaced pair of "beam mode" curves, for example in the region marked by a dotted circle on Figure 3, a complex interaction and exchange of modal characteristics takes place. Whilst the nature of this *quid pro quo* remains uncertain, what can be said is that the identity of modes 10 and 11 to the left of curve B is retained by modes 8 and 9 to the right of curve B; also, the nature of the two "edge modes" denoted on curve A by the letter X are identical to the two "edge modes" denoted further up the curve A by the letter Y. In other words, crossovers of the type just described do not alter the nature of any of the modes either side of the crossing.* Clearly, the existence of "edge" modes is very much a consequence of the completely free panel boundary conditions.

5. CONCLUSIONS

A detailed study of the vibration characteristics of completely free, open, cylindrically curved, isotropic shell panels has been undertaken by using the *h-p* version of the finite element method. The convergence properties of this shell element have been established, thereby rendering it suitable for use in the parameter studies that follow. Curves of frequency versus included angle have been obtained for the first 20 modes of panels ranging from a flat plate at one extreme, to a full, although unjoined, cylinder at the other. By fixing the panel aspect ratios a/b at $0{\cdot}5$, 1 and 2 respectively, and maintaining a constant thickness-to-length ratio h/b of 1/2000, results have been generated for a large family of shell panels.

The curves of frequency versus included angle illustrate (i) that the majority of the low frequency modes of completely free, open, curved panels, are virtually independent of shell curvature, and (ii) that the relatively few modes that are most heavily influenced by curvature effects all involve motion confined to the lengthwise edges of the panel. Similar modes have been observed for cantilevered cylindrical panels [21], and it can be concluded that the fewer the constraints on a curved panel are, the more strongly these edge modes manifest themselves.

ACKNOWLEDGMENTS

The financial assistance of EPSRC, contract number GR/J 06306, is gratefully acknowledged. The ANSYS results were computed courtesy of Mr G. S. Aglietti.

REFERENCES

1. V. S. Gontkevitch 1962 *Transactions Akademii Nauk USSR*, *Kiev*, *Laboratoriya Hidraulichnykh Mashyn*. *Sbornik Trudou*, *No*. **10**, 27–27. Free vibrations of shallow shells (in Russian).

* Within the crossover region itself, some mode re-structuring clearly will take place.

2. V. S. Gontkevitch 1964 *Natural Vibrations of Plates and Shells*. Kiev: Nauk Dumka; A. P. Filipov, editor. (Translated by Lockheed Missiles and Space Co.)
3. A. W. Leissa 1973 *Vibration of Shells* (NASA SP-288). Washington, D.C.: U.S. Government Printing Office.
4. A. W. Leissa and Y. Narita 1984 *Journal of Sound and Vibration* **96**, 207–218. Vibrations of completely free shallow shells of rectangular planform.
5. Y. Narita and A. W. Leissa 1986 *Transactions of the Americna Society of Mechanical Engineers*, *Journal of Applied Mechanics* **53**, 647–651. Vibrations of completely free shallow shells of curvilinear planform.
6. M. S. Qatu 1992 *Shock and Vibration Digest* **24**(9), 3–15. Review of shallow shell vibration research.
7. C. W. Lim and K. M. Liew 1994 *Journal of Sound and Vibration* **173**, 343–375. A *pb*-2 Ritz formulation for flexural vibration of shallow cylindrical shells of rectangular planform.
8. K. M. Liew and C. W. Lim *American Society of Civil Engineers*, *Journal of Engineering Mechanics* **121**(12), 1277–1283. Vibratory behaviour of doubly curved shallow shells of curvilinear planform.
9. K. M. Liew and C. W. Lim 1996 *Acta Mechanica* **114**(1–4), 95–119. Vibration of doubly curved shallow shells.
10. C. W. Lim, S. Kitipornchai and K. M. Liew 1997 *Journal of Vibration and Control* **3**(1), 119–143. Comparative accuracy of shallow and deep shell theories for vibration of cylindrical shells.
11. A. E. H. Love 1892 *A Treatise on the Mathematical Theory of Elasticity*. Cambridge: Cambridge University Press; first edition.
12. R. N. Arnold and G. B. Warburton 1949 *Proceedings of the Institute of Mechancial Engineers* (Series A) **167**, 62–80. The flexural vibrations of thin cylinders.
13. A. Peano 1976 *Computers and Mathematics with Applications* **2**, 211–224. Hierarchies of conforming finite elements for plane elasticity and plate bending.
14. I. Babuska, B. A. Szabo and I. N. Katz 1981 *SIAM Journal of Numerical Analysis* **18**(3), 515–545. The *p*-version of the finite element method.
15. O. C. Zienkiewicz, J. P. de S. R. Gago and D. W. Kelly 1983 *Computers and Structures* **16**(1–4), 53–65. The hierarchical concept in finite element analysis.
16. I. Babuska and B. Guo 1986 *Computational Mechanics* **1**, 21–41. The *h-p* version of the finite element method, Part 1: the basic approximation results.
17. B. W. Char, K. O. Geddes, G. H. Gonnet, B. L. Leong, M. B. Monagan and S. M. Watt 1993 *Maple V Language Reference Manual*. Berlin: Springer-Verlag.
18. ANSYS Version 5.3, 201 Johnson Road, Houston, PA 15342-1300.
19. R. S. Langley 1994 *Journal of Sound and Vibration* **169**, 43–53. The modal density and mode count of thin cylinders and curved panels.
20. N. S. Bardell 1991 *Journal of Sound and Vibration* **174**, 655–676. Chladni figures for completely free parallelogram plates: an analytical study.
21. J. K. Lee, A. W. Leissa and A. J. Wang 1983 *International Journal of Mechanical Science* **25**(5), 361–383. Vibrations of cantilevered circular cylindrical shells: shallow versus deep shell theory.